15 Computer Assisted Physics

C. Bersier, T. Mayer (since Aug. 02), P. F. Meier, E. Olbrich, S. Renold, and E. Stoll

In this report, we want to concentrate on the following research topics:

- Interpretation of the properties of high temperature superconductivity materials using spin-polarized *ab initio* calculations
- Non-linear dynamical study with particular reference to time series analysis of electroencephalograms in collaboration with two groups of the Medical Faculty

We selectively report on the charge distribution in La_2CuO_4 before and after doping (15.1.1), on the calculation of copper chemical shifts in cuprates and re-examination of Knight shift data (15.1.2), and on results of time series analysis of sleep EEG (15.2).

15.1 Electronic structure of high-T_c materials

15.1.1 Charge distribution in $La_{2-x}Sr_xCuO_4$

The parent compounds of high-T_c materials are insulators. This has been rationalized within an ionic model where the state of each atom is described by a formal valence which has an integer value. Thus, for example in La_2CuO_4 these ionic charges are La^{3+}, Cu^{2+}, and O^{2-}, respectively. Upon doping, i.e. when some La^{3+} are substituted by Ba^{2+} or Sr^{2+}, the substance becomes metallic and superconducts below the critical temperature T_c. In the ionic model the missing electrons that are introduced by doping are attributed to the planar oxygens which become O^{1-}. In the terminology of holes it is said that the intrinsic holes are on the coppers and the extrinsic holes due to doping go to the oxygens.

This view, however, is too simplistic. We therefore have performed a detailed analysis of the charge distribution in undoped and doped La_2CuO_4.

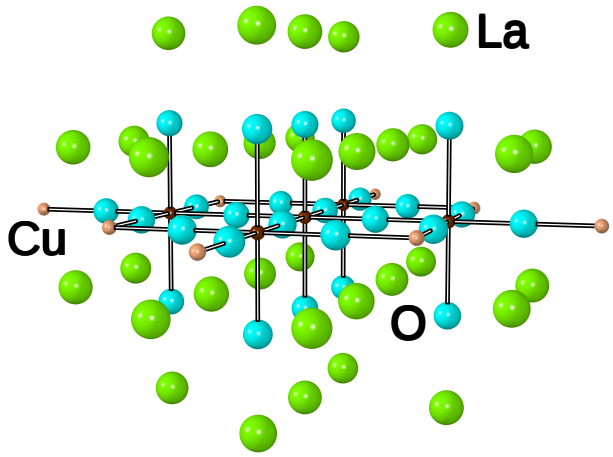

Figure 15.1: *The Cu_5O_{26}/Cu_8La_{34} cluster.*

The results are obtained for the cluster Cu_5O_{26}/Cu_8La_{34} (see Fig. 15.1) which comprises five unpaired electrons calculated with spin multiplicity M=4 which qualitatively corresponds to four spin-down electrons distributed on the four exterior coppers of the cluster and one spin-up electron on the central

copper atom, coinciding with the model of long-range antiferromagnetism observed for La_2CuO_4. The nuclear positions were fixed according to the tetragonal crystal structure. There are five Cu atoms and 26 oxygen atoms in the cluster but for the analysis of charges we select only those atoms at the center of the cluster for consideration. Those atoms close to the periphery of the cluster are not accounted for since these will include effects expected from the cluster edge.

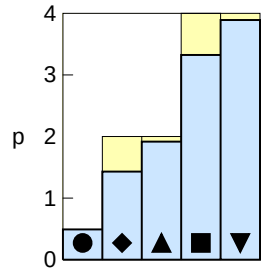

Figure 15.2: *Partial Mulliken populations (tinted blue) of the atomic orbitals for La_2CuO_4: Black symbols denote $4s$ (circles), $3d_{x^2-y^2}$ (diamonds), and $3d_{3z^2-r^2}$ (triangles up), $2 \times p(O_p(2p_\parallel))$ for the planar oxygens (squares), and $2 \times p(O_a(2p_\parallel))$ for the apical oxygens (triangles down). The yellow tinted areas denote the missing charge against the simple ionic model.*

For La_2CuO_4, the Mulliken populations p of the relevant orbitals are $p(3d_{x^2-y^2}) = 1.43$, $p(3d_{3z^2-r^2}) = 1.92$, $p(O_p(2p_\parallel)) = 1.66$, and $p(O_a(2p_\parallel)) = 1.95$ where $O_p(2p_\parallel)$ denotes the atomic orbital (AO) of the planar oxygen pointing towards the two copper neighbors and $O_a(2p_\parallel)$ is the AO of the apical oxygen directed along the z-axis. Note that all other copper $3d$ and oxygen $2p$ orbitals are effectively doubly occupied. These populations are shown in Fig. 15.2. They correspond to an "intrinsic hole content" of about 1.43, which, however, is compensated by the occupancy of the copper $4s$ orbital by $p(4s) = 0.49$.

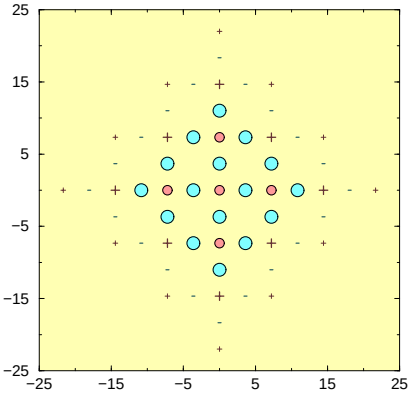

Figure 15.3: *Illustration of the peripheral charge method representing the five copper atoms (red circles), the 16 planar oxygen atoms (blue circles), and additional point charges (+ and − signs). The additional plus signs (brown) are at the locations of copper atoms and the minus signs (blue) at the locations of oxygen atoms. We have tried to indicate the relative magnitude of each charge by the size of the + and - sign symbols.*

Doping is simulated in two ways, firstly by removing an electron from the undoped cluster and changing the multiplicity from M=4 to M=3 and secondly (see Fig. 15.3) by placing additional point charges around the periphery of the cluster (the peripheral charge method).

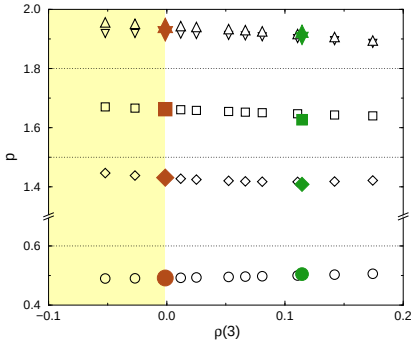

Figure 15.4: *Partial Mulliken populations of the atomic orbitals versus charge $\rho(3)$ for La_2CuO_4: $3d_{3z^2-r^2}$ (triangles down) and $2p_z$ ($O_a(2p_\parallel)$) for the apical oxygens (triangles up), $3d_{x^2-y^2}$ (diamonds) and $2p_\sigma$ ($O_p(2p_\parallel)$) for the planar oxygens (squares), and $4s$ (circles). Empty symbols refer to calculations with the peripheral charge method. The yellow area denotes an electron doped region not accessible by experiments. (The horizontal dotted lines are included to assist visibility.)*

The main interest in this dual treatment of doped clusters is to determine whether the choice of spin state crucially affects the charge distribution. In Fig. 15.4 we present the changes in the partial Mulliken populations as calculated by the peripheral charge method to simulate doping (empty symbols). The quantity $\rho(3)$ is given by $\rho(3) = \rho(\mathrm{Cu}) + 2\rho(\mathrm{O}_p) + 2\rho(\mathrm{O}_a) + 6$ and is interpreted as an approximate estimate of the number of extrinsic holes. It should be zero for the stoichiometric compound. The filled symbols in Fig. 15.4 for $\rho(3) = 0$ and $\rho(3) = 0.12$ refer to calculations on the stoichiometric cluster before and after removal of a single electron respectively. The correspondence of the two methods is surprisingly good if it is remembered that there is no spin state change in the peripheral charge method, that is all symbols refer to the M=4 spin state, whereas the filled symbols for $\rho(3) = 0.12$ refer to the M=3 spin state. Thus, the frequently used simplistic model of doping which solely removes electronic charge from the planar oxygen orbitals ($O_p(2p_{\|})$ is not entirely supported here since these results show that the apical oxygen p orbitals are affected to a similar extent. However the redistribution of charge in the copper orbitals is very significant. It has to be noted that these results are obtained with fixed nuclear positions. A change in the charges, however, invariably will lead to a change in bond lengths. To account for this effect requires extensive calculations which currently are under way.

Electric field gradients (EFG) depend sensitively on the aspherical charge distributions around the target nucleus. Experiments [1; 2] show that in $La_{2-x}Sr_xCuO_4$ the nuclear quadrupole frequency at the copper increases with increasing doping concentration x with a slope of approximately $0.8x$. This variation is partly due to a change in the lattice constant a as has been shown in Ref. [3] where $\mathrm{d}a/\mathrm{d}x \sim -0.2$ Å was estimated. The influence of the size of the lattice constant on the EFG values has been investigated in Ref. [4]. In the following the results for the calculated EFG values have been corrected for this change in a.

Figure 15.5: *Electric field gradients for the central Cu nucleus in La_2CuO_4. The dotted curve denotes ${}^{\mathrm{I}}V_{zz}$, the dashed curve is the sum ${}^{\mathrm{I}}V_{zz}+{}^{\mathrm{II}}V_{zz}$ and the full curve (with diamonds) $V_{zz} = {}^{\mathrm{I}}V_{zz}+{}^{\mathrm{II}}V_{zz}+{}^{\mathrm{III}}V_{zz}+W_{zz}$. Curves refer to calculations with the peripheral charge method and squares refer to calculations without additional point charges. Stars are experimental data [1]. The yellow area denotes an electron doped region not accessible by experiments.*

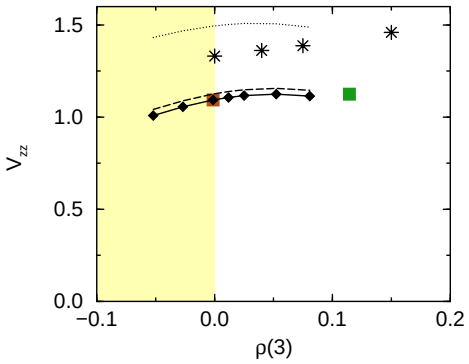

In Fig. 15.5 we represent the main EFG component V_{zz} at the copper as obtained from the simulated doping calculations. The filled squares denote the values obtained without point charges for M = 4 and, at $\rho(3) = 0.12$, for one electron removed and M = 3. The diamonds denote the results obtained with the peripheral charge method, using filled diamonds to emphasize the linear response region. Experimental data [1] for the copper quadrupole frequencies are represented by stars. For La_2CuO_4, the theoretical value is about 15 % smaller than the experiment which in view of the extreme sensitivity of the EFG on the partial occupations is still considered as a good agreement. (A redistribution of Δp of 0.02 electrons from the $3d_{3z^2-r^2}$ to the $3d_{x^2-y^2}$ AO suffices to explain this difference.) The slope of the increase of the calculated EFG with doping, however, reproduces the data astonishingly well for small doping concentrations where the peripheral charge method should be applicable.

A partitioning of the contributions to the EFG tensor V_{ij} of the target nucleus is given in the following

way

$$V_{ij} = {}^{\mathrm{I}}V_{ij} + {}^{\mathrm{II}}V_{ij} + {}^{\mathrm{III}}V_{ij} + W_{ij} \tag{15.10}$$

where the "on-site" term (I) accounts for contributions from basis functions centered at the target nucleus, the term labelled II contains mixed on-site and off-site contributions, and III and W contain purely off-site contributions (see Ref. [5] for further details). In Fig. 15.5 the contribution I is indicated by the dotted line. It is evident that the changes of the total value (full curve) are dominated by the contribution I, i.e. the changes in the partial occupations of the on-site copper orbitals. The dashed line represents the summed contributions from I and II. The difference between the dashed and the full curve thus is the "lattice contribution" ${}^{\mathrm{III}}V_{ij} + W_{ij}$ which is small and not modified upon doping. This result is of particular relevance for the interpretation of NQR data since changes in the nuclear quadrupole frequencies are often analysed in terms of changes in the "lattice contributions". The ab-initio calculations, however, demonstrate [5] that these "lattice contributions" are marginal.

15.1.2 Re-examination of NMR shifts in cuprates

In collaboration with the Department of Physical Chemistry of the University of Geneva we have extended our previous cluster calculations in La_2CuO_4 to calculate and understand the chemical shifts [6]. Chemical shielding tensors have been notoriously difficult properties to calculate with accuracy in the past but recent developments of several state-of-the-art quantum chemical methods have proved encouraging. This has enabled us to monitor the influence of the cluster size, the quality of the basis set used for the description of the atomic orbitals, and the type of gauge invariance on the calculated shielding contributions. These investigations have been used for a critical review of copper Knight shift data in cuprates.

The chemical shielding σ is a measure of the local magnetic field δH at a nucleus produced by the electronic currents under the influence of a homogeneous external magnetic field H_{ext}, i.e. $\sigma = -\Delta H / H_{ext}$. For the determination of the chemical shielding the electronic ground state is calculated and then perturbation theory is used for the induced current density and the magnetic field ΔH.

The electronic ground state is obtained self-consistently using spin-polarized density functional theory for clusters of different sizes with different basis sets formed as linear combinations of atomic orbitals into molecular orbitals (LCAO-MO). Given the ground state the chemical shielding tensor is calculated perturbation theoretically with different standard quantum chemical schemes which differ essentially in the way they choose the gauge for the magnetic field.

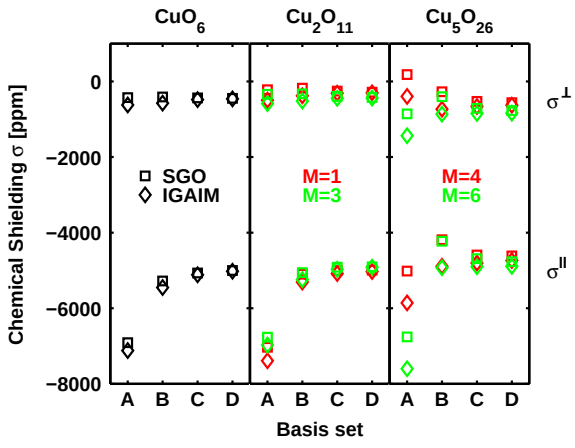

Figure 15.6: *The plot summarizes the results for the in-plane component, $\sigma^{\perp}$, (upper part) and the component parallel to the c-axis, $\sigma^{\parallel}$, (lower part) of the chemical shielding at the copper nucleus in La_2CuO_4. The left (middle, right) panel displays the results in the smallest (intermediate, largest) cluster as a function of basis set quality. The squares and the diamonds distinguish between results obtained with two different quantum chemical schemes. For the two larger clusters, calculations with different electronic spin states (multiplicity M) have been performed. They are distinguished with red and green colors.*

The calculations for the shielding constant at the copper nucleus in La_2CuO_4 [6] are summarized in Fig. 15.6. Both components, $\sigma^{\parallel}$ and $\sigma^{\perp}$, are given for clusters containing one, two, and five copper atoms (named CuO_6, Cu_2O_{11} and Cu_5O_{26}) as a function of basis set size for two different schemes and different spin states (see figure caption). It is seen that for large basis sets (C and D) the shielding become independent on all these parameters and we conclude with the following theoretical values: $\sigma^{\parallel} = -(4800 \pm 300)$ ppm and $\sigma^{\perp} = -(600 \pm 300)$ ppm.

To compare the obtained shielding constants in La_2CuO_4 to experiments one has to take into account that the measured Knight shifts are in fact differences of resonance frequencies between a target and a reference substance which - in the case of copper NMR - is the monovalent copper in CuCl. We have therefore repeated the calculations for a cluster representing CuCl.

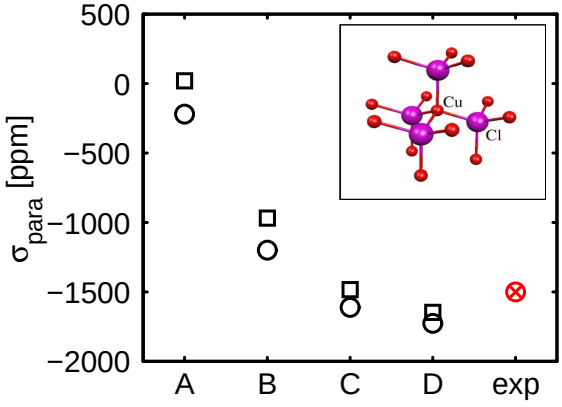

Figure 15.7: *Paramagnetic part of the shielding constant at the copper nucleus in the reference substance CuCl as a function of basis set size with quality increasing from A to D. On the right, the experimental result [7] is indicated in red. The inset shows the used cluster.*

In Fig. 15.7 the paramagnetic part of the isotropic component of the shielding tensor is given as a function of the basis set for two schemes, SGO and IGAIM. It is seen that for increasing basis set quality the results become independent on the schemes and converge to a value of $\sigma_{para} = -1700$ ppm. Its absolute value is comparable to the diamagnetic shielding of $\sigma_{dia} = 2400$ ppm.

First, we were quite surprised to get such a substantial paramagnetic contribution to the shielding constant but we then figured out that in 1978 already, NMR chemists compared the shielding of copper in the free copper ion (with - by symmetry - no paramagnetic contribution) to those in various copper compounds and found a paramagnetic shielding in CuCl of $\sigma_{para} = -1500$ ppm [7]. Thus, our theoretical result is in good agreement with the experimental value.

This result has serious consequences. The experimental data for cuprates have been explained using a perturbation theoretical formula for the paramagnetic shielding. If the reference substance itself has a substantial paramagnetic contribution to the shielding constant this formula must not be applied to the measured shifts. For a correct comparison between theory and experiment the experimental chemical shifts have to be corrected for the paramagnetic shielding of the reference substance.

We therefore suggest to use a new terminology in NMR, the paramagnetic field modification $\overline{K}_L(t) = -\sigma_{para}(t) = K_L(t-r) - \sigma_{para}(r)$, being the magnetic shift of the target with respect to the reference substance $(t-r)$ corrected for the paramagnetic shielding of the reference substance (r). This quantity has the important advantage that it is independent of the reference substance. For further details, see [6].

The Knight shift is the relative difference of the resonance frequencies of a particular nuclear magnetic moment in the target substance and in an arbitrary reference substance. It can be divided into a temperature independent chemical shift arising from the non-itinerant electrons and a spin shift arising from the electrons in the conduction band. It is assumed that the spin contribution in the superconducting state gradually vanishes as temperature is decreased due to more and more electrons

being bound in Cooper pairs. Hence, the chemical shift is identified as the magnetic shift at lowest temperatures. The connection to the shielding is as follows: the chemical shift is the difference between the shielding in the reference and the target substance.

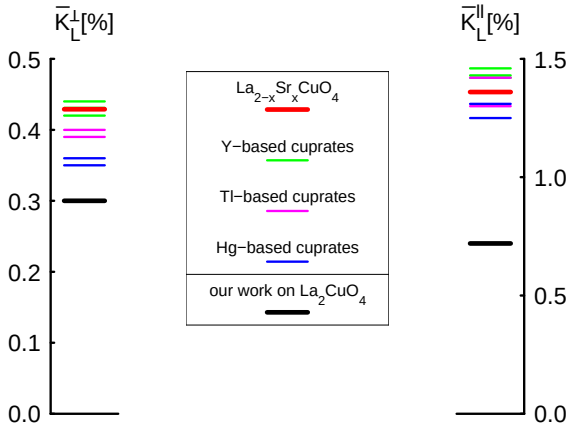

Figure 15.8: *A comparison between theoretical values in La_2CuO_4 (black) and experimental values in $La_{2-x}Sr_xCuO_4$ (red) and in various other high temperature superconducting cuprates. The left (right) side shows the paramagnetic field modification for the applied field in the plane (along the c-axis).*

In Fig. 15.8 the theoretical values for the paramagnetic field modifications (black) are compared to values extracted from experiments in the La-compound (red) and in other high-temperature superconducting cuprates. For the perpendicular component of the paramagnetic field modification the theoretical values are smaller but still in reasonable agreement with experiment. However, for the component parallel to the crystallographic c-axis there is a large discrepancy between theory and experiment. We presently investigate various explanations for this disagreement. First, we note that Zheng, *et al.*, have measured the copper magnetic shifts both in $YBa_2Cu_4O_8$[8] and in $TlSr_2CaCu_2O_{6.8}$[9] and found that they are unexpectedly appreciably field dependent and decrease with decreasing magnetic field. A correct comparison of theory and experiment, however, requires the extrapolation to zero field. Second, we emphasize that impurities in the sample lead to a non-vanishing spin contribution to the magnetic shifts even at lowest temperatures.

15.2 Time series analysis of EEG

In the previous year we continued our research on nonlinear time series analysis of EEG, which is conducted in collaboration with the institute of pharmacology and toxicology and the neurological clinic. As a next step in unravelling the character of the dynamics of the EEG we focused our research on the relationship between nonlinearity and nonstationarity. By performing a surrogate data analysis one can test, how likely the time series under study was produced by a linear system. However, if the null hypothesis is rejected this can be not only due to nonlinearity but also due to nonstationarity. We studied the question, whether the nonlinear signatures observed in the human sleep EEG previously [10] are due to a stationary nonlinear dynamics or rather are caused by nonstationary linear dynamics.

We found, that short segments of human sleep EEG with a duration ≤ 1 s are well described by linear models such as autoregressive (AR)-models and show no significant nonlinearity, while the rejection of the linearity hypothesis for longer segments can be explained by the temporal dynamics of the coefficients of these linear models. It turned out that the magnitude of their variations depends on the sleep stages. They are strongest in light sleep and less strong in slow wave and non-REM sleep.

Studying the dynamics of the coefficients of the AR-models allows to define oscillatory events, because the dynamics of an AR(p)-model is composed of m relaxators and n harmonic oscillators with $p = m + 2n$. The frequencies f_k and the damping coefficients γ_k are related to the complex poles

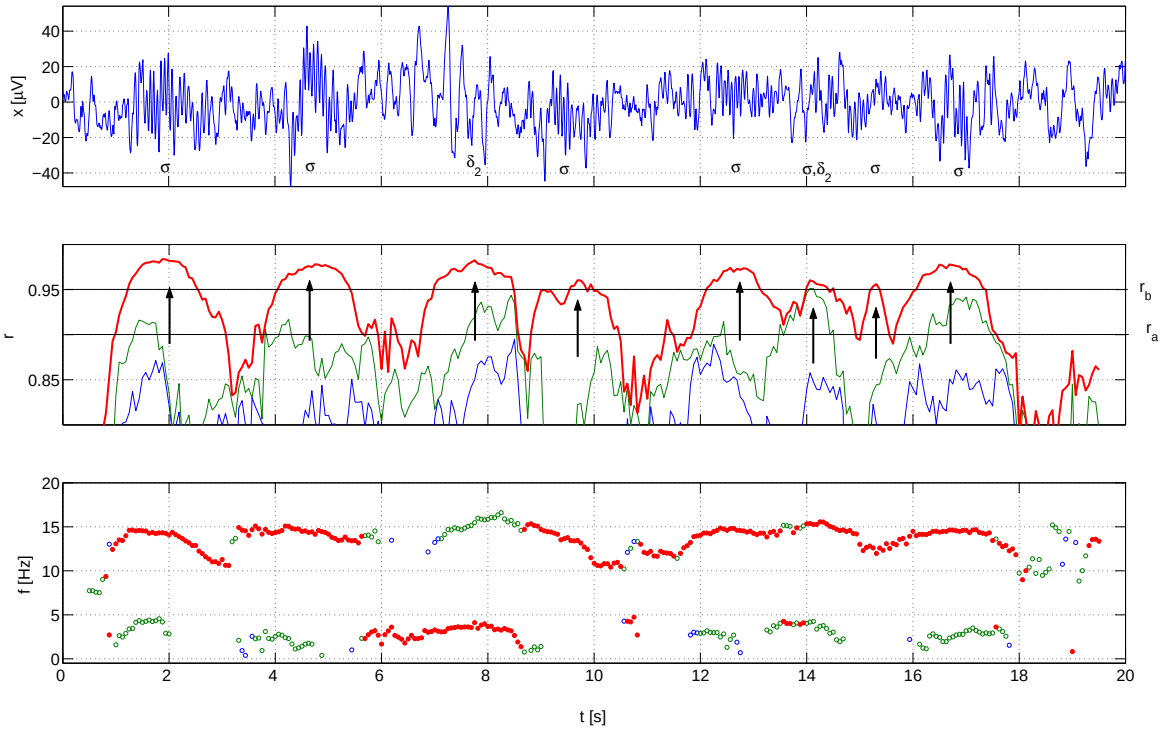

Figure 15.9: *EEG data (upper panel) with oscillatory events marked by arrows, σ-spindles and δ_2-fast delta waves. The time course of r_k and the corresponding frequencies f_k are shown in the lower panels. The pole with lowest damping is indicated by the bold red line and filled circles, the poles with the second and third lowest damping by the green and blue lines and circles, respectively.*

$z_k = r_k \exp(i\phi_k)$ of the AR-model by $f_k = (2\pi\Delta)^{-1}\phi_k$ and $\gamma_k = -\Delta^{-1} \ln r_k$ with Δ denoting the sampling time. An oscillatory event is detected, whenever the absolute value of a pole exceeds a predefined threshold r_a as illustrated in Fig. 15.9. In the shown segment both sleep spindles (marked by σ) and fast delta waves (denoted as δ_2) were detected. It turned out that this algorithm is a reliable detector for sleep spindles and, furthermore, also for alpha waves, as well as for fast and slow delta waves. Because the algorithm is model based and not a pattern recognition algorithm, it might help to identify the dynamical processes leading to the occurrence of spindles or other oscillatory events in the sleep EEG.

[1] T. Imai, C. P. Slichter, K. Yoshimura, and K. Kosuge, Phys.Rev.Lett.**70**, 1002 (1993).

[2] S. Ohsugi, Y. Kitaoka, K. Ishida, G. Zheng, and K. Asayama, J. Phys. Soc. Jpn. **63**, 700 (1993).

[3] R. L. Martin, Phys.Rev.Lett.**75**, 744 (1995).

[4] S. Renold and P. F. Meier, J. of Superconductivity, in print.

[5] E. P. Stoll, T. A. Claxton, and P. F. Meier, Phys.Rev.B, **65**, 064532 (2002).

[6] S. Renold, T. Heine, J. Weber, and P. F. Meier, Phys.Rev.B **67**, 024501 (2003).

[7] O. Lutz, H. Oehler, and P. Kroneck, *Z. Phys. A*, **288**, 17 (1978).

[8] G.-q. Zheng, W. G. Clark, Y. Kitaoka, K. Asayama, Y. Kodama, P. Kuhns, and W. G. Moulton, Phys.Rev.B **60**, R9947 (1999).

[9] G.-q. Zheng, H. Ozaki, Y. Kitaoka, P. Kuhns, A. P. Reyes, and W. G. Moulton, Phys.Rev.Lett.**88**, 077003 (2002).

[10] Y. Shen, E. Olbrich, P. Achermann, and P. F. Meier, *Clin. Neurophysiol.*, **114**, 199-209 (2003).